Design and Flight Testing of Inflatable Wings with Wing Warping

Jamey D. Jacob, Andrew Simpson, and Suzanne Smith
University of Kentucky, Lexington, KY 40506

ABSTRACT

The paper presents work on testing of inflatable wings for unmanned aerial vehicles (UAVs). Inflatable wing history and recent research is discussed. Design and construction of inflatable wings is then covered, along with ground and flight testing. Discussions include predictions and correlations of the forces required to warp (twist) the wings to a particular shape and the aerodynamic forces generated by that shape change. The focus is on characterizing the deformation of the wings and development of a model to accurately predict deformation. Relations between wing stiffness and internal pressure and the impact of external loads are presented. Mechanical manipulation of the wing shape on a test vehicle is shown to be an effective means of roll control. Possible benefits to aerodynamic efficiency are also discussed.

INFLATABLE WINGS

PREVIOUS WORK While the concept of inflatable structures for flight originated centuries ago, inflatable wings were only conceived and developed within the last few decades. While lighter-than-air vehicles also include inflatable structures, our focus herein is on inflatable structures used solely for lift generation. Various aspects of inflatable structures are discussed elsewhere [1] while a review of inflatable wing and related technologies is included in Cadogan *et al.* [2] To provide context for the results of this paper, a selection of design concepts is included below emphasizing recent developments in inflatable wings.

Inflatable wings were successfully demonstrated in the 1950s with the Goodyear Inflatoplane (Model GA-468 is shown in Figure 1 and is also on display in the Patuxent River Naval Air Museum). The 6.7 m (22 ft) wingspan air-

Figure 1: Goodyear Model GA-468 Inflatoplane.

craft was developed as a military rescue plane that could be dropped behind enemy lines to rescue downed pilots. Technology development, including delivery of dozens of aircraft, continued until the early 1970s.

The Apteron unmanned aerial vehicle with inflatable wings was developed in the 1970s by ILC Dover, Inc. The Apteron (Figure 2) had a 1.55 m (5.1 ft) wingspan, a 373 W (0.5 hp) engine, a 3.18 kg (7 lb) gross weight and was remotely-controlled via elevons mounted on the trailing edge. The Apteron was successfully flight tested, but was never put into production.

Flight tests of deployment and low-altitude (800-1,000 ft) flight of the I2000 UAV using inflatable wings were conducted in 2001 by researchers at NASA Dryden. The wings were developed by Vertigo, Inc. for the Navy as a gun launched observation vehicle . The skeleton of the wing was made of inflatable tubes, surrounded with crushable foam to provide the airfoil cross-section. After the aircraft was released, the five-foot span inflatable wing was successfully deployed in about one-third of a second. To maintain suitable wing strength and stiffness, nitrogen
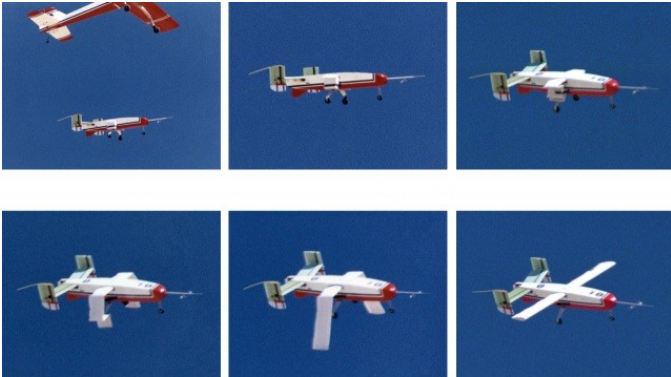
Figure 2: ILC Dover Apteron UAV.

Figure 3: In flight deployment of NASA Dryden I2000 inflatable wing.

Figure 4: Non-Inflated wing and inflated wings.

Figure 5: ILC Dovers multi-spar Inflated wing and packed configuration.

gas pressurization of 1380-1725 kPa (200-250 psi) was required. [3] The deployment is shown in Figure 3.

INFLATABLE WINGS AT UNIVERSITY OF KENTUCKY
The University of Kentucky has been working with ILC Dover, Inc. on the development and testing of inflatable wings. Two variants have been developed and tested: inflatable only wings that require constant pressurization to maintain shape and inflatable/rigidizable wings that harden into a persistent shape once inflated. The latter were tested first. UV-curable resins under development for spacecraft applications were considered for the inflatable/rigidizable wings. [2, 4, 5, 6, 7] The wings are constructed of a composite material that becomes rigid on exposure to UV light. The wings are assembled by sewing woven material to create the airfoil and internal baffling. For the inflatable/rigidizable wings, a layered material was used consisting of an external containment film, layers of resin-impregnated woven fabric selected for handling characteristics, and an internal containment layer. An inflatable urethane bladder is inserted, with long finger-like sections filling each baffle of the sewn wing. Figure 4 shows the inflatable/rigidizable wing before inflation and the wing while inflated during laboratory testing. This multi-spar design does not use foam spacer material and so packs compactly. The inflatable non-rigidizable design is shown in Figure 5. The design is similar to the rigidizable version, but does include the impregnated resin and external containment film.
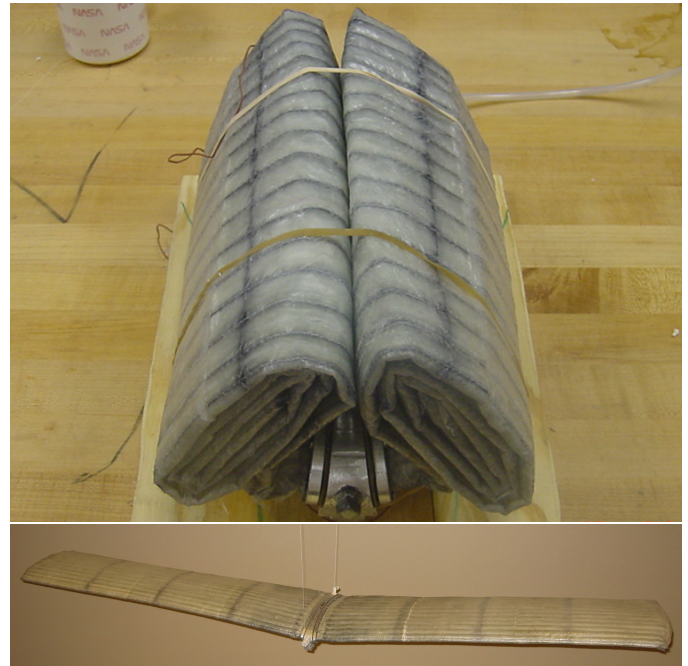
One potential application directing aspects of the development of inflatable/rigidizable wing technology is use on a "Mars Airplane." [8, 9, 10, 11] Current plans for Mars exploration include smaller Scout missions to expand the explored area. One concept under consideration is an unmanned spacecraft launched to Mars to release an aircraft designed to fly an exploratory mission over a wider range than a lander/rover and from a closer distance than an orbiter. Motivated by the requirement for a minimal packed-volume-to-weight ratio, an alternate approach for the proposed folding wing designs is an inflatable composite wing impregnated with a UV-curable resin. With this approach, wings are pressurized for deployment then rigidized with exposure to UV radiation from the sun. Once rigid, the wings no longer require pressurization to maintain their shape. [12]

Feasibility of these concepts are being tested through a series of high-altitude experiments. The flight experiments that validated this technology included three stages: 1) balloon-launched ascent to deployment altitude, 2) deployment of inflatable-rigidizable wings and

Figure 6: Recovery of second-generation inflatable/rigidizable high-altitude test article.
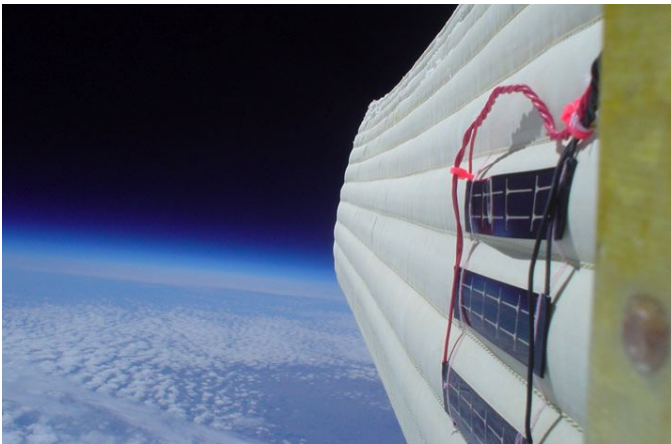

Figure 7: Inflatable wing high-altitude test article at 98,000'.

continued ascent to near 100,000 ft, and 3) release from the balloon and gliding descent under autonomous control. Note that ground-level atmospheric density on Mars is similar to that at 100,000 ft on Earth. Balloon-launched high-altitude experiments to date include the first-ever demonstration of inflatable/rigidizable wing technology on May 3, 2003 with successful deployment of inflatable wings at 55,000 ft, curing on continuing ascent to 89,603 ft and descent to recovery. [13]

More recent efforts considered tailoring the composite layering design for weight reduction. [13] A second demonstration experiment on May 1, 2004 resulted in deployment and curing of the second-generation inflatable/rigidizable wings. Figure 6 shows the test article after flight inflation and rigidization at the recovery site. Flight characteristics, aerodynamic performance, aerodynamic analysis and wind-tunnel testing for the inflatable/rigidizable wings are detailed elsewhere. [14, 15] A third flight using a Vectran non-rigidizable wing was completed on April 30, 2005 and reached altitudes of over 98,000 feet (Figure 7). Since constant gage pressure was required to maintain wing shape, the inflation system was designed to vent upon ascent and included make-up gas to maintain 185 kPa (27 psig) until landing.

WARPING INFLATABLE WINGS   The current research efforts are focused on warping an inflatable non-rigidizable wing to provide roll control through wing warping. Inflatable wings were developed by ILC Dover, Inc. which were not impregnated with the UV curable resin for use in other applications where higher wing loading is required. Since the wings do not harden, constant internal pressure is required to resist flight loads. As the wings are entirely inflatable, they do not contain ailerons. Thus, vehicles employing inflatable wings must generate a roll moment by other means. However, as the wings are non-rigid, it is possible to actively manipulate the shape of the wings to provide this roll moment.

Another motive for altering the wing shape is to improve the airfoil efficiency. Principally, efficiency is maximized by increasing the lift L and decreasing the drag D or maximizing the lift-to drag ratio (L/D) for any configuration. A given airfoil profile has vastly differing lift and drag characteristics over the possible ranges of Reynolds Number (Re) and Mach number (M). Thus, airfoils are typically designed for a narrow range of flight conditions. Alternatively, airfoils can be designed that perform adequately over a wide range of conditions, but do not perform well in any. By altering the shape of the wing, the L/D ratio can be changed across the length of the wing. Assymmetric shape changes generates differential lift between the two semi-spans while deforming the semi-spans symmetrically would provide an altered lift distribution that could be optimized for maximum L/D. The differential loading scenario can potentially be used to generate the required roll moments for the aircraft.

WING DESIGN

INFLATABLE WING CONSTRUCTION   The inflatable wing is designed such that constant internal wing pressure is required to maintain wing shape. High stiffness is achieved with low inflation pressure by maximizing inflated sectional moment of inertia. Since the wing is constructed of a flexible fabric material, it can be stowed by folding or rolling. Previous inflatable wing designs required high gage pressures to maintain wing shape. This typically requires the use of heavy seals and gaskets and thicker than desired wall thicknesses for the wing material. It also means that any leak, however small, will result in the rapid depressurization of the wing and loss of structural integrity.

The present wing design uses the presence of internal span-wise baffles or inflation cavities to help maintain structural stiffness at lower internal pressures. The outer wing (restraint) and internal baffles are constructed from high strength fibers such as Kevlar. The current incarnation as tested herein is made of Vectran, a manufactured fiber spun from Celanese Vectra liquid crystal polymer. The fibers have high-temperature resistance, high strength and modulus, and high resistance to moisture and chemicals, with good property retention in hostile environments. Since Vectran is porous, a polyurethane elas-
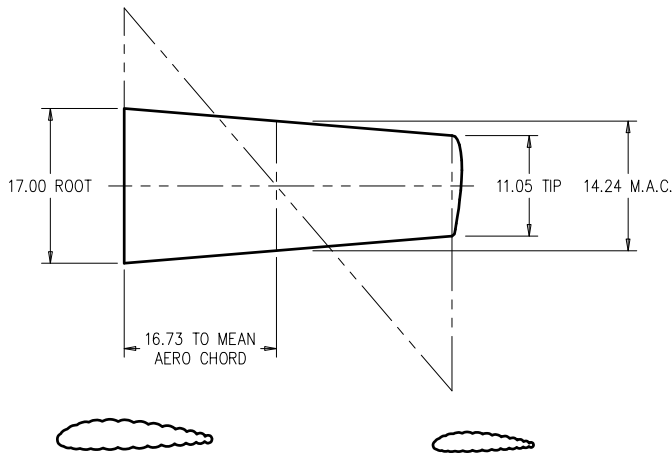
Figure 8: Planform and profile of the inflatable wing.

Figure 9: Wing deflection due to applied torsion.

tomer bladder is used to keep the internal volume pressurized. Design pressure is 186 kPa (27 psi), though the wing has been successfully flight tested at values down to 52 kPa (7.5 psi) with sufficient wing stiffness for low speed applications. The wing is constructed in semi-span sections and mounted to a plenum that can the be attached to an aircraft fuselage. The wing in both uninflated and inflated states is shown in Figure 5. The wing profile is based around a NACA 4318 with a 4 degree incidence angle. The taper ratio is 0.65 with an aspect ratio of 5.39 and a span of approximately 1.8 m (6 ft). The wing planform and root and tip cross-sections are shown in Figure 8. Note the ribbed profile and blunt trailing edge; this is discussed in more detail below. Generally, low *Re* airfoils are designed to have thin profiles. [15] Here, manufacturability dictated a thicker profile which is typically a poor performer at low *Re*. However, the airfoil actually has improved peformance in the speed regime of interest due to the roughness of the inflated profile, which has been noted in the case of bird wings, for example. [16, 17] This is discussed in more detail elsewhere. [18]

EXPERIMENTAL ARRANGEMENT

PHOTOGRAMMETRY   Full deformation measurements were made using photogrammetry. Photogrammetry unobtrusively measures spatial deformation of the wing surface. Capturing numerous digital images from a variety of positions, and referencing the images to each other allows the accurate generation of a three-dimensional representation of the wing surface. High contrast markers are placed on the surface of the wing and referenced in each image where they can be seen. The wing was then deformed into a new shape. Changes from the original shape to the new configuration can be tracked, as well as hysteresis effects, when the process is reversed. Wing surface maps can then be generated and the deflection correlated with the applied force and the internal pressure in the wing.

In order to obtain photogrammetry results, high contrast markers were placed on the surface of the wing. Higher
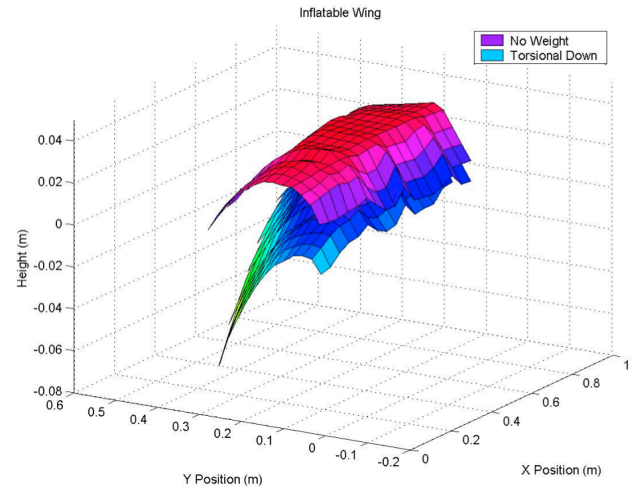
concentrations of markers were placed towards the wing tip than at the root as greater movement was expected in these areas. The markers were placed in lines from wing root to tip and from leading edge to trailing edge and a total of 243 markers were used on the top surface of the wing. Spacing between markers was approximately 1 in and each marker was 0.25 in in diameter. Additional lighting was used when capturing the images, which ensured maximum contrast. Each image was captured in such a way as to encompass all markers and occupy the entire field of view of the camera. An Olympus E-20N 5-Megapixel SLR digital camera was used to capture the images for the static measurements. Camera calibration was conducted before the image capturing process, to correct for lens distortions. The calibration results were then used to adjust the captured images for these distortions. Wing surface maps can then be generated as seen in Figure 9 where the wing is loaded under torsion similar to how the wing is deformed in flight.

STATIC DEFORMATION   Due to the novel wing design of the inflatable wing, wing stiffness is a function of inflation pressure, and thus aero-elastic behavior is a concern. To examine wing deformation, static load tests were conducted. The deflection tests were in three groups; point loads at the wing tip, distributed loading patterns, and torsional loads. In addition to simple tip deflection measurements, photogrammetry measurements were made so as to determine the deformation of an entire wing semi-span.

Figure 10 shows the deflection of the inflatable wing with a point load at the wing tip. The point load was applied at the thickest portion of the wing (approximately the 1/4 chord), where the wing has the greatest resistance to bending. Five point loads were applied (10, 20, 30, 40, and 50 N), at seven different inflation pressures ranging from approximately 34-138 kPa (5, 7.5, 10, 12.5, 15, 17.5, and 20 psi). The wing tip deflection was measured on a scale at the 1/4 chord. At the most extreme loading case (50 N)
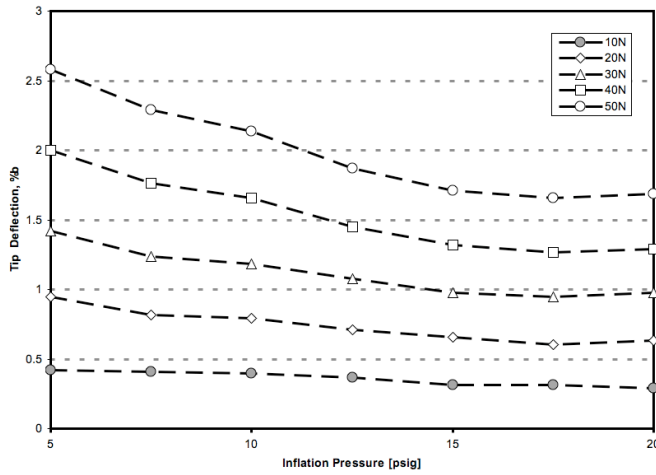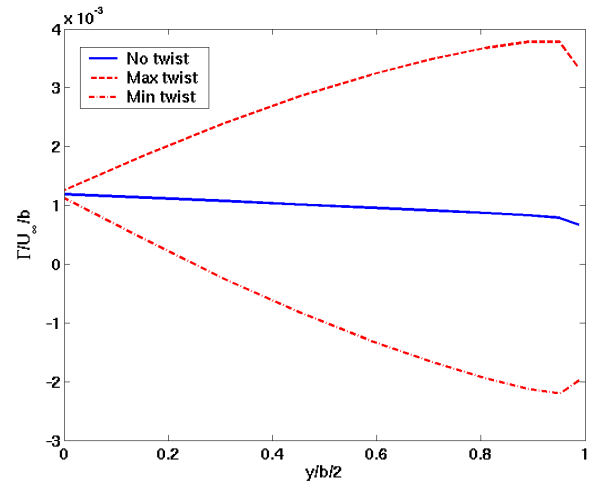
4

Figure 10: Tip deflections for point loading.

Figure 11: Undeformed (*top*) and Deformed Wing (*bottom*)

Figure 12: Lifting line prediction for the linearly twisted airfoil.

and the lowest inflation pressure (5 psi), the maximum tip deflection is less than 3% of the span.

For the distributed loading tip deflection measurements, the wing was set-up in a test stand upside down. Weight was applied on the surface in three different loading patterns and at four different internal pressures ranging from 69 to 172 kPa (10, 15, 20, and 25 psi). The loading configurations simulated flight loads under approximately 1, 2, and 2.5 g conditions. While the magnitude of the deflections change depending upon the loading conditions, the qualitative behavior is the same. Response appears to be monotonically decreasing with increasing inflation pressure. Even in the most extreme case at the highest loading and the lowest inflation pressure, the maximum tip deflection is less than 2% of the span. These results can be seen in Simpson *et al.* [19] Note that these two loading cases display similar behavior.

The wing was set-up in a test stand and was mechanically manipulated by applying a tensile force to the surface of the wing. Vectran fabric, (the same material as the wing) was bonded to the surface of the wing on the top leading edge and the bottom trailing edge of the wing. Both pieces were modified to be an attachment point for the tensile members. Thin wire was then attached and drawn taut to the opposite side of the wing at the wing base. The attachment point for the top surface wing tip, was 8 in above and 1 in behind the trailing edge of the wing. This made an angle of approximately 15° from horizontal. The attachment point for the bottom surface wing tip, was 8.5 in below and 3 in ahead of the leading edge of the wing base. This made an angle of approximately -20° from horizontal. The goal was to induce torsion in the wing from tip to root. Force transducers were connected linearly along the length of wire between these points. The transducers were connected to a DAQ that enabled real-time force measurement. The force transducers were connected to an adjustable tensioning mechanism, which could be used to adjust the force exerted. Four inflation pressures were examined: 69, 103, 138, 172 kPa (10, 15, 20, 25 psi). At each inflation pressure, five different forces (10, 20, 30, 40, and 50 N) were applied to the wing on both the top and bottom surfaces of the wing in conjunction with each other. The deformations were then measured via photogrammetry. Individual applied forces or combinations of applied forces were not examined. From measurements of typical twist deformations, seen in Figure 11, span-wise load distributions for baseline, maximum and minimum cases were generated. Placed into a lifting line code using $\alpha = 0°$, $a_o = 0.14$/radian, $\alpha_{C_l=0} = -4°$ and a tip twist of $\pm 16°$, the lift distributions are shown in Figure 12. As seen, substantial positive and negative modifications to the baseline distribution are possible.

DYNAMIC DEFORMATION   Dynamic deformation testing has taken two primary forms; smart materials and mechanical actuation. Smart materials such as piezoelectric's and shape memory alloys offer a range of potential benefits; e.g., see Kudva *et al.* [20] Piezoelectric materials have been used to alter camber, and deform lead-

Figure 13: Wing morphing using nitinol.

Figure 14: Lifting line prediction for the twisted airfoil.

ing and trailing edges. Rapid and controlled actuation of the material makes these materials desirable. However, the substantial equipment requirements for operation of these materials hampers flight testing. Shape memory alloys offer many alternatives as a wide range of shapes and actuation mechanisms exist. The wing has been warped in laboratory tests using nitinol actuators. The wing was placed in the test stand, and the nitinol attached to the wing tip trailing edge and fuselage near the root. As shown in Figure 13, the wing experiences substantial deformation under actuation. Note that under the current configuration, the trailing edge is deflected downward while the leading edge remains in the same location. When measured from leading to trailing edge at the wing tip, the twist is an effective increase in angle of attack of $3°$. If the deflection is measured from the first deformation point (approximately 0.75c), the effective flap deflection is approximately $16°$.

Mechanical actuators have also be applied to the inflatable wings. High torque servos (Hitec HSC-5998TG) mounted beneath the wing root were connected to the wing at the wing tip as outlined above. The servos are capable of delivering 14.4 kg-cm (200 oz-in) of torque at 4.8 V and actuated using a standard R/C controller. As the actuation was dynamic, photogrammetry could not be employed to monitor the shape change of the wings. Rather, videogrammetry was used to capture the dynamic shape changes to the surface of the wing. The videogrammetry system comprised of two synchronized Pulnix (M-6710CL) one mega-pixel, progressive line scan cameras. The cameras capture images at 120 frames per second. The images are then fed into Photomodeler Pro for static and dynamic measurements. The true AoA variations across the wing were then placed in a lifting line code to predict the lift from the wings. Figure 14 shows the measured AoA variation and the predicted lift generated by the variation for two cases. The twist in the wings was not linear; higher AoA deflections were measured towards
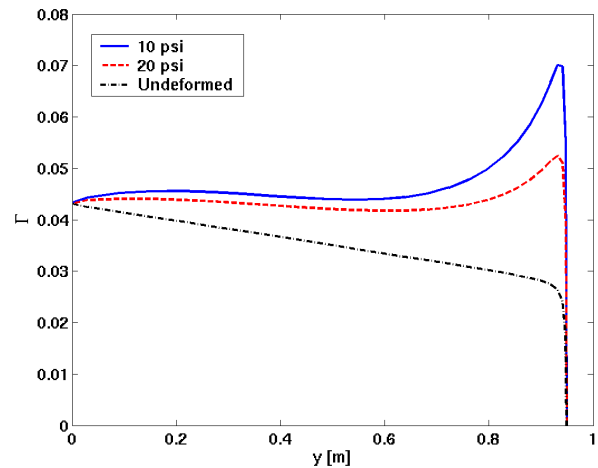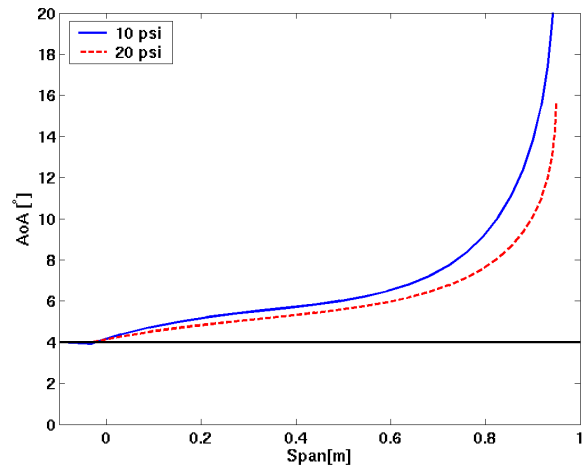
the wing tip. Note that the left hand semi-span produces nominal lift while the right hand semi-span produces increased lift as only one semi-span was warped at a time in the positive (increasing alpha) direction.

NUMERICAL ANALYSIS

Ultimately, the objective of this effort is to model the static deflection response of an inflated wing subjected to external forces applied at the tip to warp the wing for use in predicting performance. Aerodynamic loading will be added as well, but will follow the current effort. Development of an accurate finite element (FE) model for this wing is challenging. The geometry of the cross-section is intricate and changes along the span. Modeling the details of the construction, in particular the baffle seams and wing-tip closure, is not straightforward. The fabric restraint is a woven material with anisotropic properties. Finally, the structural stiffness of the wing depends on the internal pressurization. A preliminary study with a pressurized flat panel of similar material confirmed that a nonlinear static analysis is required to accurately predict the deflections resulting from pressurization.
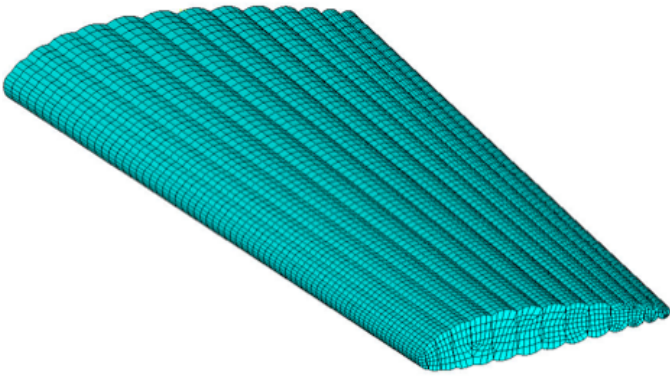
Figure 15: Meshed FASM wing model.

Material Property	Value
Fill Modulus	1.36 Msi
Warp Modulus	1.22 Msi
Shear Modulus	15 ksi
Density	8.5 oz/yd^2
Thickness	0.013 in

Table 1: Vectran material properties used in the wing model.

$P_{internal}$	δ_{ANSYS}	$\delta_{\mathrm{Measured}}$
69 kPa (10 psi)	7.7 mm (.304 in)	20 mm (.787 in)
104 kPa (15 psi)	6.9 mm (.274 in)	16 mm (.629 in)
138 kPa (20 psi)	N/A	15.5 mm (.610 in)

Table 2: Comparison of tip deflection results from model predictions and experiments.

In a previous effort, a finite element (FE) model was developed for a rigidized inflatable wing semi-span similar in cross-section design. [13] An approach for meshing the inflated cross-section and baffling was developed. Stresses resulting from steady aerodynamic loading of the fiber-glass composite semi-span were computed using a linear static analysis. The aerodynamic loading was applied as distributed pressure loads on the external surfaces of the restraint layered finite elements. The goal was optimization of the composite layering design to reduce weight and root stress levels in the rigidized wing.

A CAD model was imported into ANSYS finite element analysis software which was used to mesh the model as shown in (Figure 15). ANSYS Shell 181 shell elements were used as the primary element. These are four-node elements with six degrees of freedom per node and suitable for thin to moderately-thick shell structures. Orthotropic material properties were defined representing the different warp and fill properties of the plain weave, 53 x 53 thread count per inch, silicon-coated Vectran woven fabric material. The wing manufacturer provided data from testing of fabric samples so that the warp, fill and shear moduli could be determined. Table 1 summarizes the modulus results, along with other properties specified for the model.

Before applying external loads to the inflated wing, internal pressure was applied. Pressure loading was applied outward to the elements comprising the external surfaces to simulate the pressurization of the wings. Four different cases were considered: 69, 103, 138, and 172 kPa (10, 15, 20, and 25 psi). Nonlinear static response was computed to account for large deflections and stress stiffening. An initial model containing fewer elements did not converge for the minimum load case. Once the mesh was refined, model convergence was achieved for the smaller load cases. Higher pressures required more equilibrium iterations to converge.

After the initial pressurization analysis converged, a 50 N force was applied vertically downward at the center of the wingtip cross-section for correlation with lab deflection test data. In the experiments, deflections were measured at the point of force application. These were compared to deflections at the corresponding location in the FE model. Deflections resulting from the initial pressure load were subtracted from the final result to compare to experimental deflections at the forcing point. Table 2 summarizes the results for the different pressure cases. Figure 16 is the resulting deflected shape with 69 kPa (10 psi) inflation pressure and 50 N tip force showing, as expected, the maximum deflection at the tip and minimal deflection at the root. Model deflections are consistently less than the corresponding experimental deflections. Note that the model did not converge in the 138 kPa (20 psi) case. Further discussion is presented elsewhere. [21]

FLIGHT TESTS

For low altitude flight testing of the inflatable wings, several configurations were constructed and flown. Two have been used significantly throughout the low altitude flight tests. The first consists of a PVC fuselage with aluminum boom connected to the empennage. This configuration is shown in Figure 17. The second consists entirely of a composite fuselage of woven Kevlar fabric providing superior weight and strength. In both cases, the wings were mounted directly to the top of the fuselage while multiple tail configurations were constructed to test stability and control characteristics. These included a traditional tail, T-tail, and V-tail designs. The tail volumes are typically
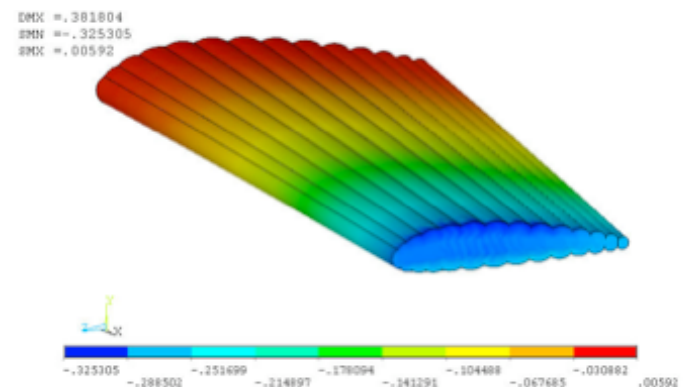

Figure 16: Deflected wing results for 69 kPa (10 psi) pressurization and a 50 N tip load.
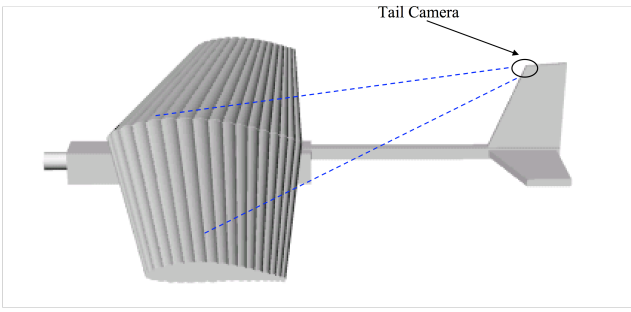
7

Figure 17: Inflatable platform.

Figure 18: Flight test with warping wing.

larger than usual to increase control at low speeds during launch. There is no aileron control on the vehicle.

For each of the test vehicles, several sets of wings were available for flight testing. In addition to sets of inflatable wings, simulated inflatable wings were constructed out of styrofoam. These wings were constructed with the same profile geometry and planform as their inflatable counterparts, and then weighted down to match the final weight of the rigidized wings. The fully inflatable wings have a mass of approximately 3 kg (6.6 lbs), including the aluminum plenum used for inflation and mounting. To achieve altitude, the vehicles were outfitted with an electric powerplant mounted in a tractor configuration. The motor was an AXI 4120 brushless motor with a Jeti controller and 24 cell battery providing up to 70 A of current. At an output of 16-20 cells and with a rated motor efficiency of greater than 82%, this provided up to 549 W of power to the propellor. Various sized folding propellers were used as needed.

To date, over 50 low altitude flight tests of various configurations have been conducted. These tests have been conducted with three goals in mind: (i) to evaluate aerodynamic performance of the morphing wings in realistic operating conditions, (ii) determine the handling characteristics of the aircraft, and (iii) to obtain appropriate feedback gains for use in an autopilot system. While aerodynamic performance closely matched that seen in the wind tunnel, handling characteristics are discussed in detail here. In general, the vehicles were very stable and exhibited slight Dutch roll at take-off due to the high dihedral.

The present vehicle employs a crude wing warping system. A standard R/C servo delivering 14.4 kg/cm (200 oz.-in.) of torque at 4.8 V, warps the wings. This is achieved through a pulley system attached to the fuselage. The servo is mounted on the tail boom located under the trailing edge of the wing on the fuselage centerline. Nylon lines are run from the servos to attachment points (similar to those used in the experiments above) on the pressure surface of the wing at the wing tip. As the servo arm rotates, one semi-span is warped down as the line tightens, while the other side slacks. Thus in the current configuration, only one semi-span is warped at a time. Additionally, the wing is warped down only, resulting in a higher than normal lift on the warped semi-span.

The UAV has been test flown in this configuration as seen in Figure 18. Two wing warping configurations have been flight tested. [19, 21] In the first, the roll and yaw of the vehicle were coupled though the R/C receiver. Qualitative flight stability was greatly improved as compared to the unwarped case. In the second configuration, the vehicle was flown without coupling the roll and yaw. Roll control was adequately provided by the wing deformation. Unfortunately, the UAV did not have any onboard sensors, thus roll rate could not be measured and correlated to servo position. A roll rate sensor has since been developed which is capable of measuring roll rate, pitch rate, longitudinal acceleration, lateral acceleration, and servo position. The results from these test flights can be used to correlate servo position (and hence wing deformation) to roll rate. Preliminary results of the flight testing of the UAV and the sensor payload with wing warping were presented elsewhere. [22]

Figure 19 shows the result of several flight tests using the onboard sensor. Each plot shows the roll rate and servo input to the wings, thus the roll rate of the aircraft should respond to the wing warping. Figure 19a shows the response of the aircraft to a step input; a nearly constant increase in roll rate (or constant roll acceleration) results, and a steady state roll rate of approximately 160°/s is seen after approximately 3 seconds. Once the servo input has been removed, the roll rate reverses until the aircraft stabilizes itself. Due to a slight asymmetry in the wings, a constant roll acceleration of approximately -0.75°/s^2 is seen without active input.

ROLL CONTROL POWER ESTIMATION   The total rolling moment can be determined from

$$C_{l_\beta} + C_{l_{\delta_r}}\delta_r + C_{l_{\delta_a}}\delta_a + C_{l_{\delta_r}}\frac{rb}{2U} + C_{l_p}\frac{pb}{2U} = \frac{1}{qSb}I_{xx}\dot{p}$$

where p is the roll rate in radians/sec, I_{xx} is the moment of inertia in roll, C_{l_p} is the roll damping coefficient, $C_{l_{\delta_a}}$ is the control power coefficient, and δ_a is the effective aileron deflection in radians. [23] Considering only a single degree of freedom and neglecting roll due to rudder deflection and sideslip, this is simplified to

$$\dot{p}\frac{I_{xx}}{qSb} - C_{l_p}\frac{pb}{2U} - C_{l_{\delta_a}}\delta_a = 0$$

8

(a) Step input.

(b) Multiple input.

(c) Corrective response.

Figure 19: Flight test with warping wing.

For a given flight, flight parameters include q, S, b, U and I_{xx} while measurable variables include p and $\dot{p}$. At initial lateral control input, we can write

$$\dot{p} = \frac{C_{l_{\delta_a}}\delta_a q S b}{I_{xx}}$$

while at steady state we have

$$\frac{pb}{2U} = \frac{-C_{l_{\delta_a}}\delta_a}{C_{l_p}}$$

The dimensionless roll-rate, $pb/2U$, is approximately 0.25. With a reported value of $I_{xx} = 0.57$ kg-m^2 ([5]), one can find that $C_{l_{\delta_a}}\delta_a = 0.0013$. Using the laboratory measured value of $\delta_a = 16°$, we estimate values of $C_{l_{\delta_a}} = 0.0047$ and $C_{l_p} = 0.0051$. This compares favorably to the predicted value of $C_{l_{\delta_a}} = 0.0053$ from McCormick. [24]

FUTURE WORK

Further work is required in numerous areas. The current wing warping system is crude and a more elegant design is needed. The nylon lines need to be attached to the surface of the wing, and not be allowed in the free-steam as is presently the case. Antisymmetrically morphing the wings will provide greater roll authority and hence greater maneuverability of the UAV. Other morphing strategies need to be examined and flight tested. Finally, all warping strategies need further ground and flight testing to quantify the improvements in lift.
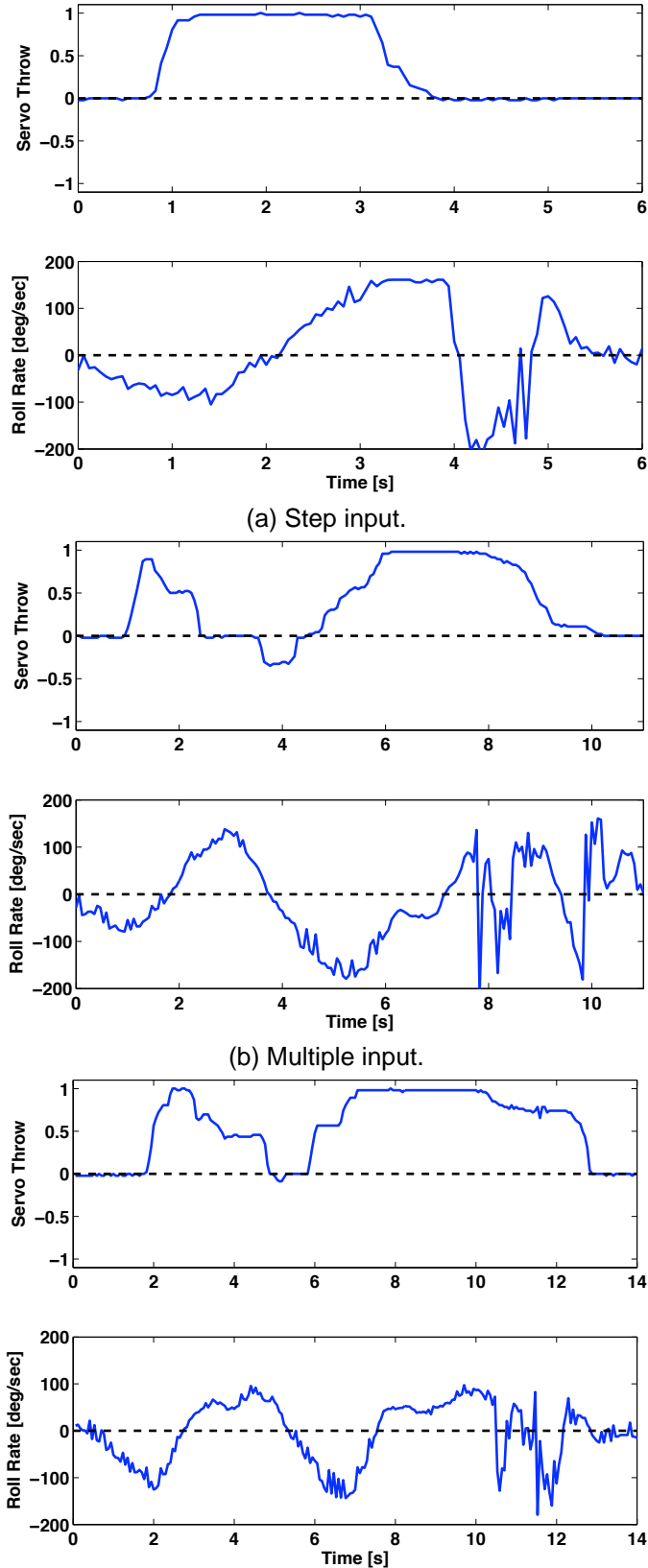
The next steps in the modeling effort will include investigating meshing and iteration options to improve convergence at higher pressures. Adjustments to modeling details will be implemented to reduce the structural stiffness for improved correlation with bending results from lab testing. Additional loading cases will be computed with different tip forces to more fully correlate the results with experimental data. Twisting loads applied near the wing tip will also be analyzed to show how the wing profile can change to modify aerodynamic properties. Additionally, the model will be modified to include a more realistic closure of the wingtip free end.

ACKNOWLEDGMENTS

REFERENCES

[1] Jenkins, C.H. (Ed.), Gossamer Spacecraft: Membrane/Inflatable Structures Technologies for Space Applications, AIAA, Washington, DC, 2001.

[2] Cadogan, D, Smith, T., Lee, R., Scarborough, S., Graziosi, D., "Inflatable and Rigidizable Wing Compo-

nents for Unmanned Aerial Vehicles," AIAA No. AIAA-2003-6630, 44th AIAA/ASME/ASCE/AHS/ASC Structures, Structural Dynamics and Materials Conference, Norfolk, VA, April 2003.

[3] Murray, J., Pahle, J., Thornton, S., Frackowiak, T., Mello, J., and Norton, B. "Ground and Flight Evaluation of a Small-Scale Inflatable-Winged Aircraft." AIAA 2002-0820, *40th AIAA Aerospace Sciences Meeting & Exhibit*, Reno, NV, Jan. 14–17, 2005.

[4] Lin, J.K., Sapna, G.H., Cadogan, D.P., Scarborough, S.E., "Inflatable Rigidizable Isogrid Boom Development," AIAA-2002-1297, 43rd AIAA/ASME/ASCE/AHS/ASC Structures, Structural Dynamics, and Materials Conference and Exhibit AIAA Gossamer Spacecraft Forum, Denver, CO: April 22-25, 2002.

[5] Cadogan, D, Smith, T., Uhelsky, F., Mackusick, M., "Morphing Inflatable Wing Development for Compact Package Unmanned Aerial Vehicles," AIAA No. AIAA-2004-1807, 45th AIAA/ASME/ASCE/AHS/ASC Structures, Structural Dynamics and Materials Conference, Palm Springs, CA, April 2004.

[6] Cadogan, D.P., Scarborough S. E. "Rigidizable Materials for Use in Gossamer Space Inflatable Structures," AIAA-2001-1417, 42nd AIAA/ASME/ ASCE/AHS/ASC Structures, Structural Dynamics, and Materials Conference and Exhibit AIAA Gossamer Spacecraft Forum, Seattle, WA: April 16-19, 2001.

[7] Allred R., Hoyt, A., Harrah, L., McElroy, P., Scarborough, S., Cadogan, D., "Light Curing Rigidizable Inflatable Wing," AIAA-2004-1809, 45th AIAA/ASME/ASCE/AHS/ASC Structures, Structural Dynamics and Materials Conference, Palm Springs, CA, April 2004.

[8] D. Hall. "Airplane for Mars Exploration: Conceptual Design of the Full-Scale Vehicle; Design, Construction and Test of Performance and Deployment Models." Final Report, David Hall Consulting, May, 1997.

[9] Smith, S.C., Hahn, A., Johnson, W., Kinnery, D., Pollitt, J., Reuther, J., "The Design of the Canyon Flyer, an Airplane for Mars Exploration." AIAA Paper 2000-0514, *38th AIAA Aerospace Sciences Meeting,* Reno, NV, Jan. 2000.

[10] Murray, J., Tartabini, P., "Development of a Mars Airplane Entry, Descent, and Flight Trajectory." NASA/TM-2001-209035, January, 2001.

[11] Guynn, M., Croom, M., Smith, S., Parks, R., Gelhausen, P., "Evolution of a Mars Airplane Concept for the ARES Mars Scout Mision." AIAA Paper 2003-6578, *2nd AIAA "Unmanned Unlimited" Systems, Technologies, and Operations Aerospace Conference*, San Diego, CA, Sep., 2003.

[12] Kearns, J., Usui, M., Smith, S., Scarborough, S., Smith, T., Cadogan, D., "Development of UV-Curable Inflatable Wings for Low Density Flight Applications,"

AIAA-2004-1503, 45th AIAA Gossamer Spacecraft Forum, Palm Springs, CA, April 2004.

[13] Usui M., Jacob, J.D., Smith, S., Scarborough, S. Cadogan, D., "Second Generation Inflatable/Rigidizable Wings for Low-Density Applications," 46th AIAA Gossamer Spacecraft Forum, Austin, TX, April 2005.

[14] Simpson, A.D., Usui, M., Smith, S.W., Jacob, J.D., "Development and Flight Testing of a UAV with Inflatable-Rigidizable Wings," AIAA-2004-1373, 42nd AIAA Aerospace Sciences Meeting and Exhibit, Reno, NV, January 2004.

[15] Simpson, A.D., Usui, M., Smith, S., Jacob, J.D., "Aeromechanics of Inflatable Wings." *AIAA 34th Fluid Dynamics Conference*, Portland, OR, June, 2004.

[16] Lissaman, P. B. S., "Low-Reynolds-Number Airfoils." *Annual Review of Fluid Mechanics,* **15**, pp. 223–39, 1983.

[17] Mueller, T., "Low Reynolds Number Aerodynamics." Springer Verlag, 1989.

[18] Santhanakrishnan, A. Jacob, J. D., "Effect of Regular Surface Perturbations on Flow Over an Airfoil", AIAA-2005-5145, *35th AIAA Fluid Dynamics Conference and Exhibit*, Toronto, Ontario, June 2005.

[19] Simpson, A.D., Santhanakrishnan, A., Jacob, J.D., Smith, S., Lumpp J., Cadogan, D., "Flying on Air: UAV Flight Testing with Inflatable Wing Technology". AIAA-2004-6570 *AIAA 3rd "Unmanned Unlimited" Technical Conference, Workshop and Exhibit*, Chicago, Illinois, September 2004.

[20] Kudva, J., Appa, K., Martin, C. A., Jardine, A. P., Sendeckyj, G., Harris, T., McGowan, A., Lake, R., "Design, Fabrication, and Testing of the DARPA / Wright Lab Smart Wing Wind Tunnel Model," Proceedings of the AIAA 38th Structures and Structural Dynamics Conference, Kissimmee, Florida, April 7-10, 1997, AIAA Paper 97-1198.

[21] Simpson, A.D., Coulombe, N., Jacob, J.D., Smith, S., "Morphing of Inflatable Wings," AIAA-2005-2110 *46th AIAA/ASME/ASCE/AHS/ASC Structures, Structural Dynamics and Materials Conference 13th AIAA/ASME/AHS Adaptive Structures Conference* Austin, Texas, April 2005

[22] Simpson, A.D., Jacob, J.D., "Aerodynamic Control of an Inflatable Wing Using Wing Warping." *AIAA 35th Fluid Dynamics Conference*, Toronto, Canada, June, 2005.

[23] Kimberlin, R., Flight Testing of Fixed-Wing Aircraft, AIAA, Reston, 2003.

[24] McCormick, B., Aerodynamics, Aeronautics, and Flight Mechanics, Wiley, New York, 1979.